A damage-friction interface model derived from micromechanical approach

Elio Sacco, Frédéric Lebon

A damage-friction interface model derived from micromechanical approach

Elio Sacco[*] - Frédéric Lebon[**]

[*]Dipartimento di Ingegneria Civile e Meccanica, Università di Cassino e del Lazio Meridionle

[**]LMA, Aix-Marseille Univ, CNRS, UPR 7051, Centrale Marseille, F-13402 Marseille Cedex 20, France

Abstract

The present paper deals with a micromechanical model of interface able to couple the damage (micro-crack) evolution, the non-penetration conditions (Signorini equations) and the friction effect (Coulomb's law). At a typical point of the interface, a Representative Volume Element (RVE) is considered; it is characterized by the presence of two different materials and by a microcrack evolving along the material discontinuity. Thus, a deductive approach based on a micromechanical analysis and on a homogenization procedure is proposed, in order to derive an imperfect, i.e. soft, interface model. In particular, the solution of the micromechanical problem on the RVE is determined considering three subproblems and properly superimposing their solutions. Then, a simplified micromechanical approach is performed by modeling the behavior of the material constituting the RVE in a very essential manner. Evolutionary laws for the crack growth are given and the equations governing the unilateral and friction phenomena are presented. In particular, the original proposed procedure is applied to derive an interface model for masonry structures considering the brick-mortar

interaction. The solutions of the three subproblems are determined adopting the finite element method on the specific RVE for different crack lengths; then, the solutions are interpolated by developing a spline technique. A numerical procedure based on the return-mapping algorithm and the classical backward-Euler integration scheme is presented for the specific considered evolutive problem. Some numerical tests, for monotonic and cyclic loadings are presented, remarking the ability of the proposed approach to reproduce the complex features of brick-mortar interfaces; comparisons between the results obtained adopting the simplified and the proposed models are performed.

Keywords: Interface, micromechanics, damage and friction, masonry.

1. Introduction

In many structural problems in mechanical and civil engineering, nonlinear phenomena occur in thin layers characterized by high strain and damage gradient, e.g. (Lorentz, 2008; Oinonen and Marquis, 2011; Parriniello et al., 2009; Salles et al., 2011; Spada and Giambanco, 2009). The behavior of these thin layers can be modeled introducing special mathematical elements, named interfaces, which are characterized by zero thickness and are governed by the relative displacements occurring between two surfaces.

The interest and the use of the interfaces in mechanics are really wide. Interfaces are adopted to model the behavior of different bodies in contact, eventually in adhesion, considering friction effects, to reproduce the growth and evolution of fractures in a body or to simulate the presence of damage or plasticity bands.

Considerable effort has been supplied in the last years on the modeling of the interface behavior. Two main problems arise in the definition of an interface model; one concerns the capability to define a model whose governing parameters are dependent on the materials which are bonded together; the other one is related to the fact that a finite (low) stiffness is associated with an element characterized by a zero thickness.

At least two different mechanical approaches are used to model these interfaces. In the first one (phenomenological), the thickness of the interface is zero and the mechanical properties are obtained from physical considerations and experiments. There exists a large class of such models. Another approach (deductive) can be developed considering the thin layer of the body material which contains the potential fracture line. This thin layer of material is named in the following as interphase. The mechanical parameters of the interface model, characterized by zero thickness, are identified on the basis of the parameters of the material (or of the materials) constituting the interphase. In fact, the dependence parameters are linear or nonlinear spring-like parameters depending on the thickness and on the mechanical behavior of the interphase. In the deduced interface model, the interfacial stress vector becomes (usually) continuous, but the displacements at either side of the interface become discontinuous, with the interfacial stress vector depending on the jump in displacement. These boundary conditions have been extensively used to model imperfect interface properties, which might lead to physically unrealistic phenomenon, such as the interpenetration at the interface.

Interface models presenting important advances on the consideration of very strongly nonlinear effects as adhesion, friction or damage has been presented by Raous et al. (1999), Del Piero and Raous (2010) and Freddi and Frémond (2006); they formulated the model in the framework of continuum thermodynamics, considering the contact zone as a material

boundary and deriving the constitutive laws by the choice of two specific surface potentials: the free energy and the dissipation potential.

Particular interest received the development and the use of interfaces in modeling the behavior of masonry elements, as it can be found for example in (Uva and Salerno, 2006) and the references therein. Interfaces are used to model fractures at macroscopic level, i.e. at the structural scale, but also to simulate the mechanical response of the masonry at the material scale. In fact, interfaces can be used to model the response of the mortar joining the bricks of the masonry or to describe the behavior of the mortar-brick interaction. In the first case, the mortar is substituted in the mathematical model of the masonry by interfaces, suitably increasing the size of the bricks. This approach has been adopted by several researchers. Among the others, Lofti and Shing (1994) proposed an interface constitutive model able to reproduce the initiation and propagation of the fracture in the mortar joints, due to the presence of normal and shear stresses and accounting for the possible dilatancy. Giambanco and Di Gati (1997) and Giambanco and Mroz (2001) formulated a simple cohesive model based on a Coulomb type yield function, with tensile cut-off and non-associative evolution law. Lourenço and Rots (1997) and, then, Oliveira and Lourenço (2004) implemented a constitutive interface model formulated in the frame of the plasticity theory, capable of simulating the cyclic behavior of the cohesive zone, reproducing the nonlinear response in the unloading phase.

Interface models are used in the context of masonry response to simulate the interaction occurring between the mortar joint and the bricks. In this framework, a model based on the adhesion intensity was developed by Fouchal et al. (2009), simulating decohesion between mortar and full or hollow bricks and the damage occurring in the mortar itself. A mortar-brick interface model, which takes the damage of the mortar joint into account, has been presented

by Pelissou and Lebon (2009), based on the material model for the mortar proposed by Gambarotta and Lagomarsino (1997). The model is derived assuming the brick-mortar interaction governed by three phases: the brick, the mortar and a thin interphase between the two materials, subjected to damage and friction. Since the interphase is thin, the interface model is recovered by performing an asymptotic analysis, as in Lebon et al. (2004) and Lebon and Zaittouni (2010).

Moreover, an interesting study in the development of interface elements consists in the derivation of a model which takes into account at the macroscopic scale the effects resulting from microscopic and mesoscopic scales; in other words, to propose multi-scale interface models. A crucial challenge is to take into account the nonlinear phenomena occurring at cracks at the microscopic scale, which are essentially the unilateral contact and the friction on the mouths of the crack as well as the evolution of this crack. A proposal in this direction has been presented by Alfano and Sacco (2006) and by Alfano et al. (2006). In these papers, the interface damage is considered governed, at a micromechanical level, by the partial decohesion due to the nucleation of micro-cracks, while the progressive interface damage corresponds to the micro-crack growth and coalescence until the formation of macro-cracks, i.e. of the fracture. These phenomena are modeled by assuming that a representative elementary area of the interface can be decomposed into an undamaged part and a completely damaged part, where a unilateral friction law is introduced. Then, the initial model has been properly modified and applied to describe the brick-mortar interface by Sacco and Toti (2010).

The objective of the present work is the development of a new procedure, based on the homogenization technique, for the derivation of an innovative and effective interface model, able to reproduce the complex features of brick-mortar interfaces. In fact, a micro-macro

interface model is proposed, which takes into account at the micro-scale non-penetration conditions, friction, sliding and crack evolution but it is characterized by reduced computational cost. The model is built on the basis of the deductive approach, considering the interphase and, then, defining a soft interface, i.e. characterized by finite stiffness (Lebon et at., 2004).

The paper is divided in four parts. In section 2, the considered interphase is introduced and the interface model is derived. In particular, the problem is studied at a microscopic level, the damage variable is defined and damage evolution laws are introduced. Section 3 is devoted to the solution technique, defining three subproblems and, also, a simplified homogenization approach is discussed. In section 4, the numerical procedure is introduced using finite elements (FE) and a classical backward-Euler integration scheme is detailed for the specific nonlinear evolutive problem under consideration. Section 5 deals with some numerical applications, developed making use of a spline regression of the FE solutions. In particular, mode I, mode II and mixed mode tests are presented and the ability of the proposed approach to reproduce the complex features of brick-mortar interfaces is remarked.

2. Interface model

2.1. Micromechanical approach

Let a typical point of the mortar-brick interface be considered. A representative volume element (RVE) at that typical point is defined as an interphase region. It is characterized by the presence of microcracks which can evolve, can be open or closed and can develop frictional stresses.

The geometry of the RVE, schematically reported in Figure 1, is determined by the height h, obtained as the sum of the thicknesses of the mortar and brick involved in the degradation

phenomenon at interphase, the length $2b$, determined as the characteristic distance between the microcracks and the width w, which depends on the size of the mortar-brick.

Following standard arguments of Continuum Damage Mechanics, the damage parameter D is introduced as ratio between the crack length $2a$ and the total size of the RVE:

$$D = a / b \tag{1}$$

Three different states can be recognized at the brick-mortar interphase, as reported in Figure 2:

- at the interface point *A*, the mortar-brick bond is absolutely undamaged,
- at the interface point *B*, partial decohesion between the two contact surfaces of the different materials occurred;
- at the interface point *C*, the decohesion phenomenon is complete.

Considering the RVE at the point *A*, the contact surfaces do not present any microcrack. The RVE associated to point *B* contains partial decohesion due to the presence of microcracks. In the RVE corresponding to point *C* the coalescence of microcracks occurred and a total decohesion is present, so that a macrocrack appears into the representative element which results completely damaged.

The relative displacement vector at the typical point of the mortar-block interface is denoted by $\mathbf{s}$. Accordingly, the RVE associated to a typical point is subjected to an overall relative displacement equal to $\mathbf{s}$. In particular, the vector $\mathbf{s}$ represents in the RVE the relative displacement between the two edges parallel to the microcrack direction, i.e. to the line of material discontinuity, as schematically illustrated in Figure 3.

With reference to Figure 3, simple geometrical evidences lead to:

$$\mathbf{s}_{B'} + \mathbf{h} + \mathbf{s} = \mathbf{h} + \mathbf{s}_{B''} \quad \Rightarrow \quad \mathbf{s} = \mathbf{s}_{B''} - \mathbf{s}_{B'} \tag{2}$$

Denoting with the subscripts $_N$ and $_T$ the components in the normal and tangential direction of the interface, respectively, according to the local coordinate system illustrated in Figure 3, the relative displacement can be written as $\mathbf{s} = \{ s_T \quad s_N \}^T$.

Note that the relative displacement $\mathbf{s}$ induces in the RVE only the average strain components $E_{NT} = s_T / h$ and $E_N = s_N / h$, i.e

$$\mathbf{E} = \{ E_{NT} \quad E_N \}^T = \mathbf{s} / h \tag{3}$$

As matter of fact, the normal strain in the direction of potential fracture is mostly neglected in the interface models.

The average shear and normal stress components in the RVE are introduced as (Hill, 1963):

$$\Sigma_{NT} = \frac{1}{V} \int_V \sigma_{NT} \, dV \quad , \quad \Sigma_N = \frac{1}{V} \int_V \sigma_N \, dV \tag{4}$$

where V represents the RVE volume, while the average of the local normal stress in the direction of potential fracture is neglected.

2.2. Interface mathematical model

In this section, the RVE at the typical point of the interface is considered. The constitutive laws for the mortar and brick materials are reported; the governing equations of the friction-contact effect are given and a damage model is illustrated.

2.2.1. Mortar and brick constitutive laws

Indeed, linear elastic constitutive laws are considered for the mortar and brick materials:

$$\boldsymbol{\sigma}^m = \mathbf{C}^m \boldsymbol{\varepsilon}^m \quad , \quad \boldsymbol{\sigma}^b = \mathbf{C}^b \boldsymbol{\varepsilon}^b \tag{5}$$

where $\mathbf{C}^m$ and $\mathbf{C}^b$ are the 3×3 isotropic elasticity matrices for the mortar and brick materials, respectively.

2.2.2. Unilateral contact and friction

Denoting by $\mathbf{d}=\{d_T \quad d_N\}^T$ the relative displacement of the crack mouths, and by τ and σ the shear and normal stresses on the crack, the following possible cases can occur:

$$\begin{aligned} &d_N>0, \quad |d_T|\geq 0, \quad \sigma=0, \quad \tau=0 \\ &d_N=0, \quad |d_T|=0, \quad \sigma<0, \quad |\tau|<\tau_0 \\ &d_N=0, \quad |d_T|\geq 0, \quad \sigma<0, \quad |\tau|=\tau_0 \end{aligned} \tag{6}$$

where τ_0 is the limit shear stress associated to the normal stress σ. The unilateral contact is governed by the conditions:

$$d_N\geq 0 \quad , \quad \sigma\leq 0 \quad , \quad d_N\,\sigma=0 \tag{7}$$

Introducing the set of admissible relative displacements at the crack mouths, $\Gamma=\{d_N : d_N\leq 0\}$, the condition (7) can be written in the equivalent form as:

$$\sigma\in\partial I_\Gamma(d_N) \tag{8}$$

where $I_\Gamma(d_N)$ is the indicator function of the set Γ, i.e.

$$I_\Gamma(d_N)=\begin{cases}0 & \text{if } d_N\geq 0\\ \infty & \text{if } d_N<0\end{cases} \tag{9}$$

The friction phenomenon can be described by means of the vector $\mathbf{p}$, representing the inelastic slip relative displacement occurring at the typical point of the crack; the evolution of $\mathbf{p}$ is assumed to be governed by the classical Coulomb yield function:

$$\phi(\tau,\sigma)=\mu\langle\sigma\rangle_- +|\tau|=\mu\sigma+|\tau| \tag{10}$$

where μ is the friction coefficient and the symbol $\langle\sigma\rangle_-$ denotes the negative part of the contact normal stress. Note that in relationship (10) it is not strictly necessary to perform the negative part of the contact normal stress, as it results $\sigma \le 0$ because of equation (8).

The following non-associated flow rule is considered for the evolution of the components of the vector $\mathbf{p}$:

$$\dot{\mathbf{p}} = \dot{\lambda} \begin{Bmatrix} \dfrac{d\phi}{d\tau} \\ 0 \end{Bmatrix} = \dot{\lambda} \begin{Bmatrix} \dfrac{\tau}{|\tau|} \\ 0 \end{Bmatrix} \tag{11}$$

together with the Kuhn-Tucker conditions:

$$\dot{\lambda} \ge 0, \quad \phi(\tau,\sigma) \le 0, \quad \dot{\lambda}\phi(\tau,\sigma) = 0 \tag{12}$$

where λ is the so-called plastic multiplier. Finally, the friction inelastic vector takes the form $\mathbf{p} = \begin{Bmatrix} p_T & 0 \end{Bmatrix}^T$. It can be remarked that, when $d_N \ge 0$ it results $\tau = 0$ and, as a consequence, from equation (10) it results $\phi(\tau,\sigma) = |\tau|$, leading to $\tau = 0$ and $p_T = \lambda = d_T$.

2.2.3. Damage evolution law

About the evolution of the damage parameter D, i.e. the crack growth, a model which accounts for the coupling of mode I of mode II of fracture is considered.

In particular, it is assumed that the damage evolution is governed by the overall relative displacement acting on the RVE. The two quantities η_T and η_N, defined as the ratios between the first cracking relative displacements s_T^0 and s_N^0 and the full crack relative displacements s_T^f and s_N^f are introduced:

$$\eta_T = s_T^0 / s_T^f \quad , \quad \eta_N = s_N^0 / s_N^f \tag{13}$$

Then, the parameter η, which relates the two modes of fracture, is defined as follows:

$$\eta = 1 - \frac{1}{\alpha^2}\left(\langle s_N \rangle_+^2 \eta_N + s_T{}^2 \eta_T \right) \tag{14}$$

where the quantity $\langle s_N \rangle_+$ is the positive part of the normal relative displacement s_N and the parameter α is evaluated according to the formula:

$$\alpha = \sqrt{\langle s_N \rangle_+^2 + \left(s_T \right)^2} \tag{15}$$

Finally, the damage parameter is assumed to be a function of the history of relative displacement as follows:

$$D = \max_{history} \left\{ \min \left\{ 1, \tilde{D} \right\} \right\} \tag{16}$$

where $\tilde{D}$ can be expressed by the relationship :

$$\tilde{D} = \frac{1}{\eta}\left(\frac{\beta}{1+\beta} \right) \tag{17}$$

with β the quantity given by the expression:

$$\beta = \sqrt{\left(\frac{\langle s_N \rangle_+}{s_{0N}} \right)^2 + \left(\frac{s_T}{s_{0T}} \right)^2} - 1 \tag{18}$$

The damage evolution law is completed by the mode I and mode II fracture energies (per unit of area) which are given by the relationships:

$$\begin{aligned} G_{cI} &= h\int_0^\infty \Sigma_N \, \delta E_N \quad = \int_0^\infty \Sigma_N \, \delta s_N \qquad \text{with } \Sigma_{NT} = 0 \\ G_{cII} &= h\int_0^\infty \Sigma_{NT} \, \delta E_{NT} = \int_0^\infty \Sigma_{NT} \, \delta s_T \qquad \text{with } \Sigma_N = 0 \end{aligned} \tag{19}$$

Different evolutionary damage laws can be adopted in the model. The use of damage laws governed by the relative displacement vector **s** leads to a crack growth which does not

depend on the contact-friction; this is a great advantage from a computational point of view, as shown in the following.

The damage evolution can be also deduced by applying the classical Linear Fracture Mechanics (LFM), whose Griffith equation gives:

$$G(a) = -\frac{\partial U(a)}{w \cdot \partial a} \quad , \quad G(a) = G_c \tag{20}$$

i.e. there is fracture evolution when the release rate energy $G(a)$ is equal to the critical fracture energy G_c; in first of the equations (20), $U(a)$ represents the internal energy of the RVE. Solving the second of equations (20), the crack length a can be determined and, as consequence, the damage parameter is deduced from formula (1).

Recalling the classical Hill's condition (Hill, 1963), which states that the volume average of an energy-like representation can be computed as the product of volume averages of stress and strain fields, it results:

$$U = \frac{1}{2}\int_V \left(\sigma_N \varepsilon_N + \sigma_{NT} \varepsilon_{NT}\right) dV = \frac{1}{2} V \left(\Sigma_N E_N + \Sigma_{NT} E_{NT}\right) \tag{21}$$

with evident meaning of the symbols. Setting:

$$U_N = \frac{1}{2} V \Sigma_N E_N \quad , \quad U_{NT} = \frac{1}{2} V \Sigma_{NT} E_{NT} \tag{22}$$

the release rate energy in mode I and mode II are defined, respectively, as:

$$G_I = -\frac{\partial}{w \cdot \partial a}\left(\frac{1}{2} V \Sigma_N E_N H\left(E_N\right)\right) \quad , \quad G_{II} = -\frac{\partial}{w \cdot \partial a}\left(\frac{1}{2} V \Sigma_{NT} E_{NT}\right) \tag{23}$$

where $H(E_N)=1$ if $E_N>0$ and $H(E_N)=0$ if $E_N\le 0$. Introducing the critical energy in mode II and mode I, G_{cII} and G_{cI}, respectively, the crack evolution law is assumed to be governed by the relationship:

$$g=\frac{G_I}{G_{cI}}+\frac{G_{II}}{G_{cII}}-1 \quad \begin{cases} <0 & \text{no fracture evolution} \\ =0 & \text{fracture evolution} \end{cases} \tag{24}$$

According to the R-curve theory, proposed by Irwin (1960) to study the crack grow in metals and, then, adopted for cementitious composites and ceramics (Cook et al., 1987; Bazant et al., 1993; Marfia and Sacco, 2001), the fracture energies G_{cI} and G_{cII} can be assumed functions of a. Considering different types of functions for G_{cI} and G_{cII}, it is possible to obtain different mechanical responses of the RVE. In particular, specific functions for $G_{cI}(a)$ and $G_{cII}(a)$ allow to recover the same response obtained using the damage model proposed above.

3. Solution procedure

In order to recover the interface model by means of the homogenization procedure, the RVE is considered subjected to the average relative displacement $\mathbf{s}$, i.e. to the average strain $\mathbf{E}$; it is required the determination of the overall average stress $\boldsymbol{\Sigma}$. To determine the solution, the problem is split in three subproblems.

3.1. Definition of the subproblems

According to the scheme illustrated in Figure 4, the overall behavior of the RVE can be obtained studying the following three problems.

- The first problem (p1) considers the RVE subjected to a relative displacement $\mathbf{s}$, i.e. to the strain $\mathbf{E}$, assuming that the relative displacement at the crack mouths is not constrained in any way; as consequence, crack opening or superposition of the material is possible. The relative displacement at the crack is denoted as $\mathbf{d}^e$.
- In the second problem (p2), the relative displacement $\mathbf{d}^c = -\mathbf{d}^e$ is prescribed between the crack mouths, while the overall relative displacement is enforced to be zero.
- Finally, in the third problem (p3), the RVE is subjected to a relative displacement $\mathbf{p} = \{ p_T \quad 0 \}^T$ at the crack mouths, corresponding to the frictional sliding, leaving the overall relative displacement equal to zero.

The solution of the three problems, p1, p2 and p3, are denoted in the following as s1, s2 and s3, respectively.

The solution of three linear elastic problems allows to evaluate:

Solution	s1	s2	s3
Average strain	**E**	**0**	**0**
Average stress	$\boldsymbol{\Sigma}^e$	$\boldsymbol{\Sigma}^c$	$\boldsymbol{\Sigma}^f$
Stress at the crack	**0**	$\tau^c \ \sigma^c$	$\tau^f \ \sigma^f$
Relative displacement at crack	$\mathbf{d}^e$	$\mathbf{d}^c = -\mathbf{d}^e$	$\mathbf{p} = \{ p_T \quad 0 \}^T$

where the framed quantities are prescribed. By simple superposition of the three solutions, it is possible to recover any possible mechanical situation.

3.2. Possible mechanical situations

3.2.1. Open crack

If the crack is open, the solution of the problem is s1:

Average strain	Average stress	Stress at the crack	Relative displacement at crack
$\mathbf{E}$	$\boldsymbol{\Sigma} = \boldsymbol{\Sigma}^e$	$\tau = 0 \quad \sigma = 0$	$\mathbf{d} = \mathbf{d}^e$

3.2.2. Closed crack with no-sliding

If the crack is closed and no-sliding occurs at the crack mouths, the solution of the problem is s1+s2:

Average strain	Average stress	Stress at the crack	Relative displacement at crack
$\mathbf{E}$	$\boldsymbol{\Sigma} = \boldsymbol{\Sigma}^e + \boldsymbol{\Sigma}^c$	$\tau = \tau^c \quad \sigma = \sigma^c$	$\mathbf{d} = \mathbf{0}$

3.2.3. Closed crack with sliding

If the crack is closed and sliding occurs at the crack mouths, the solution of the problem is s1+s2+s3:

Average strain	Average stress	Stress at the crack	Relative displacement at crack
$\mathbf{E}$	$\boldsymbol{\Sigma} = \boldsymbol{\Sigma}^e + \boldsymbol{\Sigma}^c + \boldsymbol{\Sigma}^f$	$\tau = \tau^c + \tau^f \quad \sigma = \sigma^c + \sigma^f$	$\mathbf{d} = \mathbf{p} = \{ p_T \quad 0 \}^T$

Note that, in this case, the average strain can be considered as the sum of two quantities $\mathbf{E} = \mathbf{E}^e + \mathbf{P}$, where $\mathbf{E}^e$ and $\mathbf{P}$ represent the overall elastic and friction inelastic part of the strain, respectively. The overall inelastic part of the strain is evaluated as the average strain which leads to zero average stress when the relative displacement at crack is equal to $\mathbf{p}$:

Average strain	Average stress	Relative displacement at crack
$\mathbf{P}$	$\boldsymbol{\Sigma} = \boldsymbol{\Sigma}^e + \boldsymbol{\Sigma}^c + \boldsymbol{\Sigma}^f = \mathbf{0}$	$\mathbf{d} = \mathbf{p}$

(25)

3.3. Determination of the solutions

3.3.1. Solution s1

The solution s1 is determined prescribing the average strain $\mathbf{E}$ and enforcing zero stresses at the crack mouth. The overall stress and the relative displacement at the crack are evaluated by the relationships:

$$\boldsymbol{\Sigma}^e = \mathbf{C}\,\mathbf{E} \quad , \quad \mathbf{d}^e = \mathbf{D}\,\mathbf{E} \tag{26}$$

where the overall elastic matrix matrix $\mathbf{C}$ and the localization $\mathbf{D}$ matrix of the relative displacement at crack mouths are determined solving the following two linear elastic problems:

Prescribe		**Compute**	
Average strain	**Stress at the crack**	**Overall elastic matrix**	**Localization matrix for the relative displacement**
$E_{NT}=1$	$\tau=0$	$C_{TT}=\Sigma_{NT}$	$D_{TT}=d_T^e$
$E_N=0$	$\sigma=0$	$C_{NT}=\Sigma_N$	$D_{NT}=d_N^e$
$E_{NT}=0$	$\tau=0$	$C_{TN}=\Sigma_{NT}$	$D_{TN}=d_T^e$
$E_N=1$	$\sigma=0$	$C_{NN}=\Sigma_N$	$D_{NN}=d_N^e$

Note that, contrarily to the matrix $\mathbf{C}$, $\mathbf{D}$ is function of the position of the point along the crack; in fact, once the average strain $\mathbf{E}$ is assigned, it is possible to evaluate the relative displacement at any point of the crack mouths.

3.3.2. Solution s2

The solution s2 is determined prescribing the relative displacement field $\mathbf{d}^c=-\mathbf{d}^e$ between the crack mouths and enforcing the average strain $\mathbf{E}$ equal to $\mathbf{0}$. The overall stress and the shear and normal stresses at the crack are evaluated by the relationships:

$$\mathbf{\Sigma}^c=\mathbf{C}^c\mathbf{E} \quad , \quad \tau^c=\left(\mathbf{T}^c\right)^T\mathbf{E} \quad , \quad \sigma^c=\left(\mathbf{S}^c\right)^T\mathbf{E} \tag{27}$$

where the overall contact matrix $\mathbf{C}^c$ and the localization vectors $\mathbf{T}^c$ and $\mathbf{S}^c$ of the stresses at the crack mouths are determined solving the following two linear elastic problems:

Prescribe		**Compute**	
Relative displacement	**Average strain**	**Overall elastic matrix**	**Localization matrix for the relative displacement**
$d_T^c=-d_T^e=-D_{TT}$	$E_{NT}=0$	$C_{TT}^c=\Sigma_{NT}^c$	$T_T^c=\tau^c$
$d_N^c=-d_N^e=-D_{TN}$	$E_N=0$	$C_{NT}^c=\Sigma_N^c$	$S_T^c=\sigma^c$

$d_T^c = -d_T^e = -D_{NT}$	$E_{NT} = 0$	$C_{TN}^c = \Sigma_{NT}^c$	$T_N^c = \tau^c$
$d_N^c = -d_N^e = -D_{NN}$	$E_N = 0$	$C_{NN}^c = \Sigma_N^c$	$S_N^c = \sigma^c$

3.3.3. Solution s3

The solution s3 is determined prescribing the relative displacement field $\mathbf{d}^f = \left\{ u^f \quad 0 \right\}^T$, characterized by an assumed distribution of the tangential relative displacement between the crack mouths, and enforcing the average strain $\mathbf{E}$ equal to $\mathbf{0}$. The overall stress and the shear and normal stresses at the crack are evaluated by the relationships:

$$\boldsymbol{\Sigma}^f = \lambda \mathbf{C}^f \quad , \quad \tau^f = \lambda T^f \quad , \quad \sigma^f = \lambda S^f \tag{28}$$

where λ is set such that $d_T^f = \lambda u^f$ with

$$\max \left| u^f \right| = 1 \tag{29}$$

and the overall friction vector $\mathbf{C}^f$ and the localization scalars T^f and S^f of the stresses at the crack mouths are determined solving the following the linear elastic problem:

Prescribe		**Compute**	
Relative displacement	**Average strain**	**Overall elastic matrix**	**Localization matrix for the relative displacement**
$u^f = 1$	$E_{NT} = 0$ $E_N = 0$	$C_T^f = \Sigma_{NT}^f$ $C_N^f = \Sigma_N^f$	$T^f = \tau^f$ $S^f = \sigma^f$

Note that the relative displacement $\mathbf{d}^f$ represents the friction sliding occurring on the crack mouths; in other words, it results: $\mathbf{d}^f = \mathbf{p}$.

3.3.4. Remark

All the quantities are computed for the three considered subproblems assuming fixed the crack length, i.e. for a given value of the damage variable D. As a consequence, they have to be implicitly considered all functions of the damage.

On the base of equations (26)-(28), the overall inelastic strain defined by relationships (25) can be computed as:

$$\boldsymbol{\Sigma} = \mathbf{C}\,\mathbf{P} + \mathbf{C}^c\mathbf{P} + \lambda\mathbf{C}^f = \mathbf{0} \qquad \Rightarrow \qquad \mathbf{P} = -\lambda\left(\mathbf{C} + \mathbf{C}^c\right)^{-1}\mathbf{C}^f \tag{30}$$

where $\lambda = p_T$.

3.4. Simplified approach

A direct approach can be recovered assuming a drastic simplification of the material behavior constituting the RVE. In fact, the continuous model is substituted with a simple mechanistic model obtained considering springs in the normal and tangential direction as schematically illustrated in Figure 5. Let K_{Nm} and K_{Nb} be the stiffnesses of the mortar and brick springs, respectively, in the normal direction; while K_{Tm} and K_{Tb} denote the stiffnesses of the mortar and brick springs, respectively, in the tangential, i.e. shear, direction.

Recalling that $E_{NT} = s_T / h$ and $E_N = s_N / h$ and introducing the equivalent stiffness as:

$$K_N = \frac{K_{Nb} \cdot K_{Nm}}{K_{Nb} + K_{Nm}} \quad , \quad K_T = \frac{K_{Tb} \cdot K_{Tm}}{K_{Tb} + K_{Tm}} \tag{31}$$

it can be set:

$$K_N = \frac{\hat{C}_{NN}}{h} \quad , \quad K_T = \frac{\hat{C}_{TT}}{h} \tag{32}$$

where $\hat{C}_{TT}$ and $\hat{C}_{NN}$ denote the normal and shear stiffnesses of the undamaged interface, respectively.

3.4.1. Solution s1

The solution s1 of the simplified problem is determined evaluating the components of the overall elastic matrix $\mathbf{C}$ and of the localization matrix $\mathbf{D}$, as:

$$\begin{aligned} &C_{TT} = (1-D)\hat{C}_{TT}, \quad C_{NN} = (1-D)\hat{C}_{NN}, \quad C_{TN} = C_{NT} = 0 \\ &D_{TT} = h, \qquad\qquad D_{NN} = h, \qquad\qquad D_{TN} = D_{NT} = 0 \end{aligned} \tag{33}$$

3.4.2. Solution s2

According the solution s2 of the simplified problem, the components of the overall contact matrix $\mathbf{C}^c$ and of the localization vectors $\mathbf{T}^c$ and $\mathbf{S}^c$ are:

$$\begin{aligned} &C^c_{TT} = D\hat{C}_{TT}, \quad C^c_{NN} = D\hat{C}_{NN}, \quad C^c_{TN} = C^c_{NT} = 0 \\ &T^c_T = \hat{C}_{TT}, \qquad S^c_N = \hat{C}_{NN}, \qquad T^c_N = S^c_T = 0 \end{aligned} \tag{34}$$

3.4.3. Solution s3

The relative displacement field $\{u^f \quad 0\}^T$, characterized by an uniform distribution of the tangential relative displacement, is prescribed between the crack mouths. This condition is obtained in the simplified model assuming u^f as uniform along the crack mouths; in particular, it is set $u^f = 1$. Then, the solution s3 gives:

$$\begin{aligned} &C^f_T = -D\hat{C}_{TT}, \quad C^f_N = 0 \\ &T^f = -\hat{C}_{TT}, \qquad S^f = 0 \end{aligned} \tag{35}$$

It can be remarked that the simplified model leads to the model proposed by Alfano and Sacco (2006).

4. Numerical procedure

A numerical-discrete time integration scheme is adopted to solve the nonlinear evolution equations governing the interface behavior. The time integration is performed adopting a classical backward-Euler integration procedure. The time interval of interest is subdivided in sub-increments and the evolutive problem is solved into a typical interval $[t_n, t_{n+1}]$, being $t_{n+1} > t_n$. For brevity of notation, the subscript n denotes the quantities evaluated at the time t_n, while subscript is omitted for all quantities evaluated at the time t_{n+1}.

Once the solution at the time t_n is known as well as the strain vector $\mathbf{E} = \mathbf{s}/h$ at time t_{n+1}, the stress is computed from the strain variables by means of the return-map procedure.

The following average quantities on the crack are introduced:

- average elastic relative displacement:

$$\bar{\mathbf{d}}^e = \int_0^a \mathbf{d}^e dx_T = \left(\int_0^a \mathbf{D}\, dx_T \right) \mathbf{E} = \bar{\mathbf{D}}\, \mathbf{E} \tag{36}$$

- average contact normal and tangential stresses:

$$\begin{aligned} \bar{\tau}^c &= \int_0^a \tau^c dx_T = \left(\int_0^a \mathbf{T}^c\, dx_T \right)^T \mathbf{E} = \left(\bar{\mathbf{T}}^c \right)^T \mathbf{E} \\ \bar{\sigma}^c &= \int_0^a \sigma^c dx_T = \left(\int_0^a \mathbf{S}^c\, dx_T \right)^T \mathbf{E} = \left(\bar{\mathbf{S}}^c \right)^T \mathbf{E} \end{aligned} \tag{37}$$

- average friction normal and tangential stresses:

$$\begin{aligned} \bar{\tau}^f &= \int_0^a \tau^f dx_T = \lambda \int_0^a T^f\, dx_T = \lambda \bar{T}^f \\ \bar{\sigma}^f &= \int_0^a \sigma^f dx_T = \lambda \int_0^a S^f\, dx_T = \lambda \bar{S}^f \end{aligned} \tag{38}$$

It can be remarked that, when the model governed by equations (13)-(18) is considered, the damage evolution problem can be solved independently from the contact and friction problem, as the model assumes that the damage variable D, i.e. a, depends directly on the overall relative displacement components s_T and s_N. Thus, once the strain $\mathbf{E}$ is given at time t_{n+1}, the damage can be directly evaluated by means of equations (13)-(18). Of course, the damage is an internal variable, i.e. it is a history variable; thus, at the actual time step, the equation (16) takes the specific form:

$$D = \max\left\{D_n, \min\left\{1, \tilde{D}\right\}\right\} \tag{39}$$

When the Linear Fracture Mechanics approach is considered, the damage evolution is governed by equation (24). According to the LFM, an initial damage is assumed, so that the value of the crack length is different from zero since the beginning of the analysis. Note that if LFM is considered, the crack evolution is coupled with contact-friction effects; thus, in order to evaluate the possible growth of the crack length, it is necessary to solve the contact and friction problem.

The solution algorithm can be developed considering two possible situations: the crack is open or the crack is closed; in the second case, again two cases can arise: there is sliding or not.

4.1. Open crack

If $\bar{d}_N^e > 0$ then there is no contact and the solution at actual time step t_{n+1} is: overall average strain $\mathbf{E}$, overall average stress $\mathbf{\Sigma} = \mathbf{\Sigma}^e$, stresses on the crack mouths $\tau = 0$ $\sigma = 0$, relative displacement along the crack $\mathbf{d} = \mathbf{d}^e$.

If the LFM damage evolution is considered, formulas (23) are rewritten in the explicit form:

$$G_{II} = -\frac{\partial}{w \cdot \partial a}\left(\frac{1}{2} V \left(C_{NT} E_{NT} + C_{NN} E_N\right) E_{NT}\right)$$
$$G_I = -\frac{\partial}{w \cdot \partial a}\left(\frac{1}{2} V \left(C_{TT} E_{NT} + C_{TN} E_N\right) E_N\right) \qquad (40)$$

Assuming at the time t_{n+1} the crack length equal to a_n (predictor phase), a trial value of a fracture release rate $\tilde{g}$, defined on the base of relation (24), is computed as:

$$g = -\frac{V}{2 \cdot w}\left[\frac{C_{TT}' E_{NT} + C_{TN}' E_N}{G_{cI}} E_N H\left(E_N\right) + \frac{C_{NT}' E_{NT} + C_{NN}' E_N}{G_{cII}} E_{NT}\right] - 1 \qquad (41)$$

where the symbol prime $'$ indicates the derivative with respect to the crack length a. If g is lower than zero, there is no crack evolution, so that $a = a_n$. On the contrary, if g is less or equal to zero, there is crack evolution, so that the actual value of the crack length is determined solving, with respect to a, the algebraic equation (corrector phase):

$$\frac{C_{TT}' E_{NT} + C_{TN}' E_N}{G_{cI}} E_N H\left(E_N\right) + \frac{C_{NT}' E_{NT} + C_{NN}' E_N}{G_{cII}} E_{NT} + \frac{2 \cdot w}{V} = 0 \qquad (42)$$

4.2. Closed crack

If $\bar{d}_N^e \le 0$ then there is contact; the solution at actual time step t_{n+1} is obtained by means of a predictor-corrector algorithm.

For a given value of the crack length a, the friction trial step is evaluated as: overall average strain $\mathbf{E}$, overall average stress $\mathbf{\Sigma}^{trial} = \mathbf{\Sigma}^e + \mathbf{\Sigma}^c + \mathbf{\Sigma}^{f,trial}$, average stresses on the crack mouths $\bar{\tau}^{trial} = \bar{\tau}^c + \bar{\tau}^{f,trial}$ $\bar{\sigma}^{trial} = \bar{\sigma}^c + \bar{\sigma}^{f,trial}$, relative displacement along the crack $\mathbf{d}_n = \left\{\lambda_n \; u^f \quad 0\right\}^T$, where it is $\mathbf{\Sigma}^{f,trial} = \lambda_n \mathbf{C}^f$, $\bar{\tau}^{f,trial} = \lambda_n \bar{T}^f$ and $\bar{\sigma}^{f,trial} = \lambda_n \bar{S}^f$. The trial value of the yield function (10) is computed as:

$$\phi^{trial} = \phi\left(\bar{\tau}^{trial}, \bar{\sigma}^{trial}\right) = \mu\bar{\sigma}^{trial} + \left|\bar{\tau}^{trial}\right| = \mu\left(\bar{\sigma}^{c} + \lambda_n \bar{S}^{f}\right) + \left|\bar{\tau}^{c} + \lambda_n \bar{T}^{f}\right| \tag{43}$$

If the trial yield function is lower than zero, i.e. $\phi^{trial} < 0$, the trial state is solution of the problem; thus, it results $\boldsymbol{\Sigma} = \boldsymbol{\Sigma}^{trial}$, $\bar{\tau} = \bar{\tau}^{trial}$ and $\bar{\sigma} = \bar{\sigma}^{trial}$.

On the contrary, if the yield function is not lower than zero, i.e. $\phi^{trial} \geq 0$, the solution of the problem has to be evaluated by a correction phase. In fact, a new value of the parameter $\lambda = \lambda_n + \Delta\lambda$ is computed solving the following yield equation with respect to $\Delta\lambda$:

$$0 = \mu\left[\bar{\sigma}^{c} + \left(\lambda_n + \Delta\lambda\right)\bar{S}^{f}\right] + \left|\bar{\tau}^{c} + \left(\lambda_n + \Delta\lambda\right)\bar{T}^{f}\right| \tag{44}$$

Remarking that $\bar{\tau} / \left|\bar{\tau}\right| = \bar{\tau}^{trial} / \left|\bar{\tau}^{trial}\right|$, from equation (44) it results:

$$0 = \mu\bar{\sigma}^{trial}\frac{\bar{\tau}^{trial}}{\left|\bar{\tau}^{trial}\right|} + \bar{\tau}^{trial} + \Delta\lambda\left(\mu\bar{S}^{f}\frac{\bar{\tau}^{trial}}{\left|\bar{\tau}^{trial}\right|} + \bar{T}^{f}\right) \tag{45}$$

Multiplying all the terms by $\bar{\tau}^{trial} / \left|\bar{\tau}^{trial}\right|$, it is:

$$0 = \mu\bar{\sigma}^{trial} + \bar{\tau}^{trial}\frac{\bar{\tau}^{trial}}{\left|\bar{\tau}^{trial}\right|} + \Delta\lambda\left(\mu\bar{S}^{f}\frac{\bar{\tau}^{trial}}{\left|\bar{\tau}^{trial}\right|} + \bar{T}^{f}\right)\frac{\bar{\tau}^{trial}}{\left|\bar{\tau}^{trial}\right|} \tag{46}$$

i.e.:

$$0 = \phi^{trial} + \Delta\lambda\left(\mu\bar{S}^{f}\frac{\bar{\tau}^{trial}}{\left|\bar{\tau}^{trial}\right|} + \bar{T}^{f}\right)\frac{\bar{\tau}^{trial}}{\left|\bar{\tau}^{trial}\right|} \tag{47}$$

which leads to:

$$\Delta\lambda = -\frac{\phi^{trial}}{\left(\mu\bar{S}^{f} + \bar{T}^{f}\frac{\bar{\tau}^{trial}}{\left|\bar{\tau}^{trial}\right|}\right)} \tag{48}$$

Finally, the solution at actual time step t_{n+1} corresponding to the prescribed value of the overall average strain $\mathbf{E}$ is the overall average stress $\mathbf{\Sigma} = \mathbf{\Sigma}^e + \mathbf{\Sigma}^c + \mathbf{\Sigma}^f$ and the average stresses on the crack mouths $\bar{\tau} = \bar{\tau}^c + \bar{\tau}^f$ $\bar{\sigma} = \bar{\sigma}^c + \bar{\sigma}^f$, relative displacement along the crack $\mathbf{d} = \left\{ \left(\lambda_n + \Delta\lambda \right) u^f \quad 0 \right\}^T$, where it is $\mathbf{\Sigma}^f = \left(\lambda_n + \Delta\lambda \right) \mathbf{C}^f$, $\bar{\tau}^f = \left(\lambda_n + \Delta\lambda \right) \bar{T}^f$ and $\bar{\sigma}^f = \left(\lambda_n + \Delta\lambda \right) \bar{S}^f$.

If the LFM damage evolution is considered, taking into account the equations reported in subsection 3.3, formulas (23) are rewritten in the explicit form:

$$\begin{aligned} G_{II} &= -\frac{1}{2} V \frac{\partial}{w \cdot \partial a} \left[\left(C_{NT} + C_{NT}^c \right) E_{NT} + \left(C_{NN} + C_{NN}^c \right) E_N + \lambda C_N^f \right] E_{NT} \\ G_I &= -\frac{1}{2} V \frac{\partial}{w \cdot \partial a} \left[\left(C_{TT} + C_{TT}^c \right) E_{NT} + \left(C_{TN} + C_{TN}^c \right) E_N + \lambda C_T^f \right] E_N \end{aligned} \tag{49}$$

so that, according to condition (24), the fracture evolves when:

$$\begin{aligned} 0 = &-\frac{V}{2 \cdot w} \frac{\left(C_{NT}{}' + C_{NT}^c{}' \right) E_{NT} + \left(C_{NN}{}' + C_{NN}^c{}' \right) E_N + \lambda C_N^f{}'}{G_{cII}} E_{NT} \\ &-\frac{V}{2 \cdot w} \frac{\left(C_{TT}{}' + C_{TT}^c{}' \right) E_{NT} + \left(C_{TN}{}' + C_{TN}^c{}' \right) E_N + \lambda C_T^f{}'}{G_{cI}} E_N - 1 \end{aligned} \tag{50}$$

Equation (50) reveals that, as announced above, the damage and friction problems are coupled when LFM is employed, as the value of λ can be determined only after solving the friction problem. The splitting solution strategy is adopted, solving iteratively the problems of the damage evolution, taking frozen the value of λ, and of the friction-contact, taking frozen the value of D.

5. Numerical applications

Some numerical applications are developed in order to assess the ability of the proposed model and the developed procedure to simulate the behavior of the brick-masonry interface.

Initially, the geometry and the mechanical properties of the materials constituting the RVE are introduced. With reference to Figure 1, the geometry of the RVE is defined by the following data:

$$h_m = 2 \text{ mm}, \quad h_b = 3 \text{ mm}, \quad b = 25 \text{ mm}$$

while the mechanical properties of the brick and mortar are:

$$E_m = 1000 \text{ MPa}, \quad \nu_m = 0.15, \quad E_b = 16000 \text{ MPa}, \quad \nu_b = 0.15$$

Because of the symmetry of the RVE, the micromechanical computations are performed considering only one half of the RVE, discretized adopting a regular finite element mesh, such that each element is square with the side length equal to 1 mm. The adopted mesh is illustrated in Figure 6.

5.1. Preliminary computations

The formal vector $\mathbf{S}$ collecting the matrices $\mathbf{C}$ and $\mathbf{D}$, related to the solution s1, the matrix $\mathbf{C}^c$ and the vectors $\mathbf{T}^c$ and $\mathbf{S}^c$, related to the solution s2, the vector $\mathbf{C}^f$ and of the scalars T^f and S^f, related to the solution s3, is introduced, i.e.:

$$\mathbf{S} = \left\{ \mathbf{C} \quad \mathbf{D} \quad \mathbf{C}^c \quad \mathbf{T}^c \quad \mathbf{S}^c \quad \mathbf{C}^f \quad T^f \quad S^f \right\} \tag{51}$$

Clearly, the vector $\mathbf{S}$ is function of the crack length. In the following, all the components of $\mathbf{S}$ are computed for different values of a, adopting finite element schemes. Thus, denoting by a_1, a_2, .., a_m the m different crack lengths considered, the vectors $\mathbf{S}_1$, $\mathbf{S}_2$, .., $\mathbf{S}_m$ are

determined. In order to derive the analytical functions for all the quantities collected in the formal vector $\mathbf{S}$, spline interpolations are performed.

5.1.1. Determination of the solution s1

In Figure 7 and in Figure 8, the overall elastic moduli along the transversal (shear) and normal direction versus the crack length a are plotted.

It can be remarked that the variation of the overall elastic moduli C_{TT} and C_{NN} with respect to a is linear when the simplified model is considered.

Finally, because of the symmetry of the RVE, the values of $C_{NT} = C_{TN}$ results always equal to zero.

In Figure 9 and in Figure 10, the plot of the components of the matrix $\mathbf{D}$ are reported for different values of the crack length a, i.e. for different level of the damage state. Note that for $a = 25\,\text{mm}$, it results $D_{TT} = 5$, $D_{NT} = 0$, $D_{TN} = 0$ and $D_{NN} = 5$.

In Figure 11, the plot of the average values of the non zero components of the matrix $\bar{\mathbf{D}}$, i.e. $\bar{D}_{TT}$ and $\bar{D}_{NN}$, computed using the formula (36), are plotted versus the crack length a with diamond symbols. In the same Figure, the spline regression and the values determined using the simplified model are also plotted with a continuous line and with a dashed-dotted line, respectively. According to the simplified model, a constant value for both $\bar{D}_{TT}$ and $\bar{D}_{NN}$ is obtained.

Note that the computations are performed considering only one half of the symmetric RVE; thus, even if the values of D_{TN} and D_{NT} are not zeros for the typical value of the crack length,

on the two hales of the RVE they assume opposite values, so that their average on the whole RVE is zero, i.e. $\bar{D}_{TN} = \bar{D}_{NT} = 0$.

5.1.2. Determination of the solution s2

In Figure 12 and in Figure 13, the variations of the overall contact parameters C^c_{TT} and C^c_{NN} along the transversal (shear) and normal direction, respectively, are reported versus the crack length a. In the Figures, the values of C^c_{TT} and C^c_{NN}, computed performing finite element micromechanical analyses are reported using diamond symbols; in the same figures, the spline regression and the simplified model results are also reported. The values of $C^c_{NT} = C^c_{TN}$ results always equal to zero.

It can be simply noted that the following relationships hold true:

$$\begin{aligned} C_{TT}(a) + C^c_{TT}(a) &= C_{TT}(0) = C^c_{TT}(b) \\ C_{NN}(a) + C^c_{NN}(a) &= C_{NN}(0) = C^c_{NN}(b) \end{aligned} \tag{52}$$

Then, micromechanical analyses are performed for different values of the crack length in order to compute the contact stress parameters T^c_T and S^c_T as a function of a. The determined values of T^c_T and S^c_N are plotted in Figure 14 versus the crack length. In the same Figure the spline regression and the values obtained adopting the simplified model are also plotted. It can be remarked that, because of the symmetry of the chosen RVE, the contact stress parameters T^c_N and S^c_T are equal to zero.

5.1.3. Determination of the solution s3

The relative displacement field $\{u^f \quad 0\}^T$ is prescribed between the crack mouths; the displacement distribution is set such that the maximum absolute value, occurring at

$x_T = 25\,\text{mm}$, is set as $\max\left|u^f\right| = 1$. The relative displacement distributions to prescribe are determined for each crack length a, considering a uniform tangential stress along the crack mouths. The problems for the different lengths of the crack are solved by finite element method. The solution in terms of relative displacements is reported in Figure 15.

In Figure 16(a), the variation of the overall contact moduli C_T^f along the transversal (shear) direction is reported. In the Figure, the values of C_T^f, computed performing finite element micromechanical analyses are reported using diamond symbols; in the same figures, the spline regression and the simplified model solution are also reported. Note that, because of the symmetry of the chosen RVE, the overall contact parameter C_N^f is always equal to zero.

Then, micromechanical analyses are performed in order to compute the contact stress localization parameter T^f. The determined values of T^f are plotted in Figure 16(b) versus the crack length a. In the same figures the regression function and the simplified model solution are also plotted. Because of the symmetry of the chosen RVE, the parameter S^f is always equal to zero.

5.2. Overall interface response

Computations are developed in order to investigate the ability of the proposed micromechanical model in reproducing the effects of the damage, friction and unilateral contact of the interface. To this end, Mode I, Mode II and mixed Mode tests for monotonic and cyclic loading conditions are illustrated in the following. The aim of this section is the assessment of the ability of the proposed approach to reproduce the complex features of brick-mortar interfaces

The mechanical parameters adopted for the computations are reported in Table 1.

For the simplified model the values of s_T^0 and s_N^0 are properly modified in order to recover the same fracture energy.

5.2.1. Mode I tests

Initially, two simple mode I tests are performed. The loading histories are defined in order to perform a monotonic and a cyclic test; in fact, in the first case the maximum normal relative displacement $s_N = 0.05\,\text{mm}$ is reached, setting $s_T = 0$, while in the second case a loading history is assigned for the normal relative displacement, setting $s_T = 0$. In particular, the two loading histories, named as h1_I and h2_I, are defined as reported in Table 2.

The results for the considered monotonic and cyclic loading conditions for normal relative displacement are reported in Figure 17(a) and Figure 17(b), respectively, in terms of the overall normal stress Σ_N versus the normal relative displacement s_N. Results are given comparing the response of the proposed model with the simplified one.

5.2.2. Mode II tests

Then, two mode II fracture tests are performed. Analogously to the mode I case, even for mode II, monotonic and cyclic loading histories are investigated, denoted as h1_II and h2_II, respectively. In particular, the considered loading histories are defined as detailed in Table 3.

The results for the considered monotonic and cyclic loading conditions for shear relative displacement are reported in Figure 18(a) and Figure 18(b), respectively, in terms of the overall shear stress Σ_T versus the shear relative displacement s_T. The comparison between the results obtained adopting the proposed and the simplified models are given.

5.2.3. Mixed mode test

Finally, a mixed mode test is performed. In particular, the interface is initially subjected to a compressive stress induced by prescribing a negative value of the normal relative displacement s_N, which remains constant during the whole loading history, while a cyclic history is performed for the shear relative displacement s_T. The loading history is reported in Table 4.

In Figure 19, the plot of the overall shear stress Σ_T versus the shear relative displacement s_T is given for the proposed and simplified model.

5.2.4. Discussion of the results

Concerning the Mode I tests, it can be remarked that the simplified model well captures the overall response of the interface for monotonic as well as for cyclic loading histories. Nevertheless, slightly differences in the mechanical behavior of the proposed and the simplified model can be remarked mainly looking at the monotonic loading history, where it is well clear that the simplified model presents a linear softening branch and a higher value of the maximum stress.

For the cyclic load history, the progressive damage of the interface can be remarked; moreover, when the reverse load is applied, the recovery of the initial stiffness, due to the unilateral effect modeling the closure of the crack, occurs.

Concerning the Mode II tests, it can be remarked that, for a given value of the full crack relative displacement s_T^f and of the mode II fracture energy, the simplified model presents a linear softening branch and a higher value of the maximum shear stress with respect to the proposed model.

As for the cyclic loading history, the comparison between the results obtained by the proposed and simplified model show the quite good agreement between the two models. The progressive damage of the interface can be noted, which of course is not recovered when the reverse load is applied.

Concerning the mixed mode test, it can be remarked that the differences between the two discussed models are limited in the initial cohesive response of the interface, i.e. during the damage evolution phase.

The illustrated results show that both the models are able to couple the damage evolution with the friction effect and are able to reproduce the typical behavior of the brick-mortar interface. More specifically, the response of the mixed mode test is characterized by:

- OA: loading phase characterized by linear stress-strain response;
- AB: loading phase with nonlinear response due to the damage activation and development of friction effect;
- BC: unloading phase characterized by linear response;
- CD: unloading phase during which the damage is less than 1 and it remains constant; thus, along the crack length, friction effect is present and, because the damage is not total, a kind of hardening effect arises;
- DE: reloading phase characterized by linear response, i.e. there is not damage nor friction slip evolution;
- EF: reloading phase analogous to the phase CD; there is not damage evolution, but friction slip effect;

- FG: loading phase with nonlinear response due to the damage activation and development of friction effect; at the point G, the damage reaches its maximum value, i.e. $D = 1$;
- GH: loading phase with nonlinear response due to development of friction effect;
- HI: unloading phase characterized by linear response;
- IJ: unloading and reverse loading phase during which the friction slip decreases to zero and then becomes negative;
- JK: reloading phase characterized by linear response;
- KL: reloading phase during which the friction slip increases until zero at point L.

A quite different response can be noted for the two models in the nonlinear branch A-G, i.e. when both the damage and the friction evolve. In fact, the proposed model allows to reach higher values of the shear stress than the simplified model; this effect is due to a different coupling between damage and friction in the two models. Moreover, it can be argued that, as the fracture energy governing the damage evolution is the same in the two cases, the difference is due to the frictional effect, which in the simplified model is as underestimated.

When the interface is completely damaged and only the friction governs the interface behavior, there are not differences between the results of the two models.

6. Conclusions

A micromechanical and homogenization procedure has been proposed to derive an interface model able to reproduce the behavior of an interphase consisting in two thin layers of different materials jointed together. Fracture evolution is considered in the joining surface, where also unilateral contact, due to the crack closure, and friction effect are accounted for.

The nonlinear micromechanical problem is solved considering three linear subproblems and suitably combining their solutions.

The developed numerical procedure has been used to investigate on some simple but interesting examples. In particular, the interface constitutive law of a brick-mortar joint of a masonry is derived, implementing the proposed micromechanical and homogenization procedure. The procedure has been also applied to a simplified scheme of the RVE.

Results are carried out for mode I, mode II and mixed mode of fracture; in the latter case, the nonlinear response of the interface is shown and the damage-friction interaction is remarked. Cyclic loading histories show the gradual degradation of the interface and, for the mixed mode tests, the role played by the damage-friction coupling.

Numerical applications demonstrate the ability of the proposed micro-macro model and of the implemented numerical procedure to reproduce the complex features of brick-mortar interfaces .

The proposed procedure represents a rational way to derive the interface constitutive law. The model takes into account the damage evolution, the unilateral effect and the frictional slip, and their coupling and interaction are obtained from micromechanical considerations without introducing any external assumption at the macroscale.

Acknowledgements:. The financial support of the Ecole Centrale de Marseille and of the Consorzio RELUIS (Department of Civil Protection) is gratefully acknowledged.

References

Alfano G., Marfia S., Sacco E., 2006, A cohesive damage–friction interface model accounting for water pressure on crack propagation. Comput. Methods Appl. Mech. Engrg. 196, 192–209.

Alfano G., Sacco E., 2006, Combining interface damage and friction in a cohesive-zone model. Int. J. Numer. Meth. Engng. 68, 542–582.

Bazant ZP, Jarusek M., 1993, R-curve modeling of rate and size e_ects in quasibrittle fracture. Int. J. Fracture 62, 355–373.

Cook R.F., Fairbanks C.J., Lawn B.R., Mai Y.W., 1987, Crack resistance by interfacial bridging: its role in determining strength characteristics. Journal Material Research 2, 345–356.

Del Piero G, Raous M, 2010, A unified model for adhesive interfaces with damage, viscosity, and friction. Eur. J. Mech. A/Solids 29: 496-507.

Fouchal F., Lebon F., Titeux I., 2009, Contribution to the modelling of interfaces in masonry construction. Constr. Build. Mater. 23, 2428–2441.

Freddi F., Frémond M., 2006, Damage in domains and interfaces: a coupled predictive theory, J. Mech. Mater. Struct. , 1, 1205–1234.

Gambarotta L., Lagomarsino S., 1997, Damage models for the seismic response of brick masonry shear walls. Part I: the mortar joint model and its applications, Earthq. Eng. Struct. Dyn. 26, 423–439.

Giambanco G., Di Gati L., 1997, A cohesive interface model for the structural mechanics of block masonry. Mech. Res. Commun. 24, 503-512.

Giambanco G., Mroz Z., 2001, The interphase model for the analysis of joints in rock masses and masonry structures. Meccanica 36, 111–130.

Hill R., 1963, Elastic properties of reinforced solids: some theoretical principles. J Mech Phys Solids 11, 357–372.

Irwin G.R., 1960, Structural Mechanics, Pergaman Press, London.

Lebon F., Rizzoni R., Ronel-Idrissi S., 2004, Asymptotic analysis of some non-linear soft thin layers, Comput. Struct. 82, 1929–1938.

Lebon F., Zaittouni F., 2010, Asymptotic modelling of interfaces taking contact conditions into account: Asymptotic expansions and numerical implementation, Int. J. Eng. Sci. 48, 111-127.

Lofti H.R., and Shing P.B., 1994, Interface Model Applied to Fracture of Masonry Structures. J. Struct. Eng.-ASCE 120, 63-80.

Lorentz E., 2008, A mixed interface finite element for cohesive zone models, Comput. Methods Appl. Mech. Engrg., 198, 317–320.

Lourenço P.B., Rots J., 1997, A multi-surface interface model for the analysis of masonry structures. J. Eng. Mech. Div.-ASCE, ASCE 123, 660-668.

Marfia S., Sacco E., 2001, A fracture evolution procedure for cohesive materials, Int. J. Fracture 110, 241–261.

Oinonen A., Marquis G., 2011 A parametric shear damage evolution model for combined clamped and adhesively bonded interfaces, Eng. Fract. Mech., 78, 163-174.

Oliveira D.V., Lourenço P.B., 2004, Implementation and validation of a constitutive model for the cyclic behaviour of interface elements. Comput. Struct. 82, 1451–1461.

Parrinello F., Failla B., Borino G., 2009, Cohesive–frictional interface constitutive model, Int. J. Solids Struct., 46, 2680-2692.

Pelissou C., Lebon F., 2009, Asymptotic modeling of quasi-brittle interfaces. Comput. Struct. 87, 1216–1223.

Raous M., Cangémi L., Cocu M., 1999, A consistent model coupling adhesion, friction, and unilateral contact Comput. Methods Appl. Mech. Engrg. 177, 383-399.

Sacco E., Toti J., 2010, Interface elements for the analysis of masonry structures. Int. J. Comput. Methods Eng. Sci Mech., Vol. 11, 354-373.

Salles L., Blanc L., Thouverez F., Gouskov A.M., 2011, Dynamic analysis of fretting-wear in friction contact interfaces, Int. J. Solids Struct., 48, 1513-1524.

Spada, G. Giambanco, P. Rizzo, 2009, Damage and plasticity at the interfaces in composite materials and structures, Comput. Methods Appl. Mech. Engrg., 198, 3884-3901.

Uva G., Salerno G., 2006, Towards a multiscale analysis of periodic masonry brickwork: A FEM algorithm with damage and friction, Int. J. Solids Struct., 43, 3739-3769.

Nomenclature

RVE	representative volume element
h	height of the RVE
$2b$	length of the RVE
w	width of the RVE
$2a$	crack length
D	damage parameter
$\mathbf{s}$	relative displacement vector
E_{NT}, E_N	shear and normal average strain components of the vector $\mathbf{E}$
Σ_{NT}, Σ_N	shear and normal average stress components of the vector $\mathbf{\Sigma}$
$\mathbf{\Sigma}^e$	average stress vector for the subproblem s1
$\mathbf{\Sigma}^c$	average stress vector for the subproblem s2
$\mathbf{\Sigma}^f$	average stress vector for the subproblem s3
V	RVE volume
$\mathbf{C}^m$, $\mathbf{C}^b$	constitutive matrices for the mortar and brick materials
$\mathbf{d}$	relative displacement vector along the crack mouths
$\mathbf{d}^e$	relative displacement vector along the crack mouths for the problem p1
τ, σ	shear and normal stresses on the crack
τ^c, σ^c	shear and normal stresses on the crack for the problem p2
τ^f, σ^f	shear and normal stresses on the crack for the problem p3
I_Γ	indicator function of the set Γ
$\mathbf{p}$	inelastic slip relative displacement
$\phi(\tau,\sigma)$	Coulomb yield function
μ	friction coefficient
s_T^0, s_N^0	first cracking relative displacements
s_T^f, s_N^f	full crack relative displacements
G_{cI}, G_{cII}	mode I and mode II fracture energies
G_c	critical fracture energy
$G(a)$	elease rate energy
$U(a)$	internal energy
$\mathbf{C}$	overall elastic matrix of the RVE
$\mathbf{D}$	localization matrix of the relative displacement vector along the crack mouths for the problem p1
$\mathbf{C}^c$	overall matrix for the problem p2

$\mathbf{T}^c$	localization vector of the shear stress along the crack mouths for the problem p2
$\mathbf{S}^c$	localization matrix of the normal stress along the crack mouths for the problem p2
$\mathbf{C}^f$	overall vector for the subproblem s3
T^f	localization function of the shear stress along the crack mouths for the problem p3
S^f	localization function of the normal stress along the crack mouths for the problem p3
$\mathbf{P}$	overall inelastic strain
K_N, K_T	shear and normal stiffnesses for the simplified model

Captions of the Figures

Figure 1: Geometry of the RVE.

Figure 2: Micromechanical scheme of interface mortar-block.

Figure 3: Kinematics at macro- and micro- scale.

Figure 4: Schemes

Figure 5: Simplified scheme for the RVE.

Figure 6: Finite element mesh for the heterogeneous RVE, with microcrack.

Figure 7: Variation of the overall elastic coefficient C_{TT} as function of the crack length a.

Figure 8: Variation of the overall elastic coefficient C_{NN} as function of the crack length a.

Figure 9: First column of the matrix D versus x_T for different values of the crack opening a.

Figure 10: Second column of the matrix D versus x_T for different values of the crack opening a.

Figure 11: Average values and spline interpolation of $\bar{D}_{TT}$ (a) and $\bar{D}_{NN}$ (b) versus the crack opening a.

Figure 12: Variation of the overall elastic coefficient $C^e{}_{TT}$ as function of the half crack length a.

Figure 13: Variation of the overall elastic coefficient $C^c{}_{NN}$ as function of the half crack length a.

Figure 14: Variation of the contact coefficients $T^c{}_T$ (a) and $S^c{}_N$ (b) vs the crack length a.

Figure 15: Tangential relative displacement fields u^f to prescribe for each value of the half crack length a.

Figure 16: Variation of the contact stress parameters C^f_T (a) and T^f (b) vs the half crack length a.

Figure 17: Normal stress vs normal relative displacement for monotonic (a) and cyclic (b) loading conditions.

Figure 18: Shear stress vs shear relative displacement for monotonic (a) and cyclic (b) loading conditions.

Figure 19: Cyclic loading history for the mixed mode fracture test.

Figures

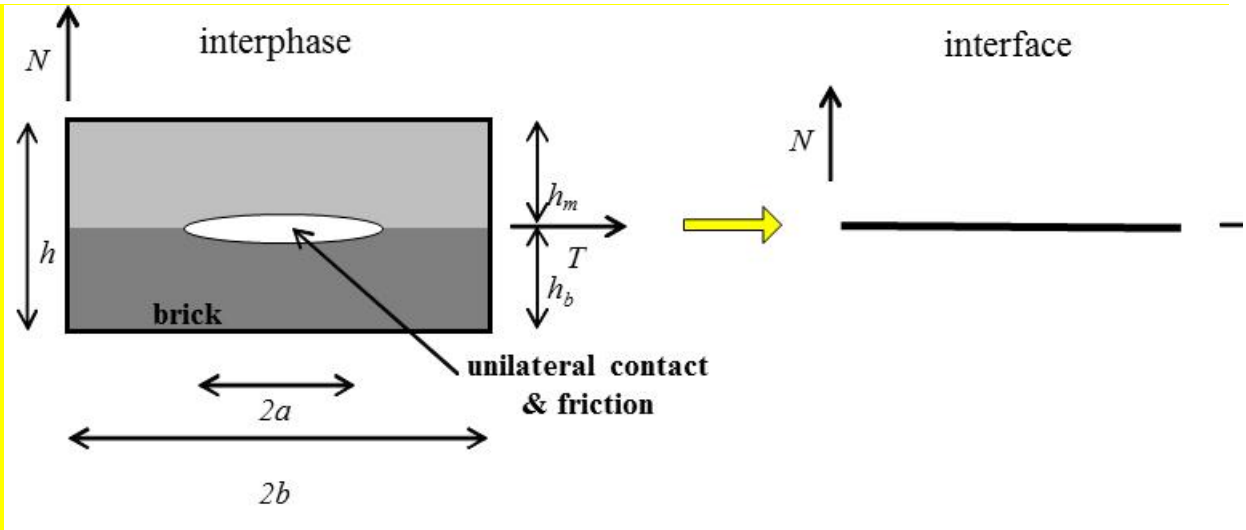

(a) (b)

Figure 1: Geometry of the RVE interphase (a) and brick-masonry interface (b).

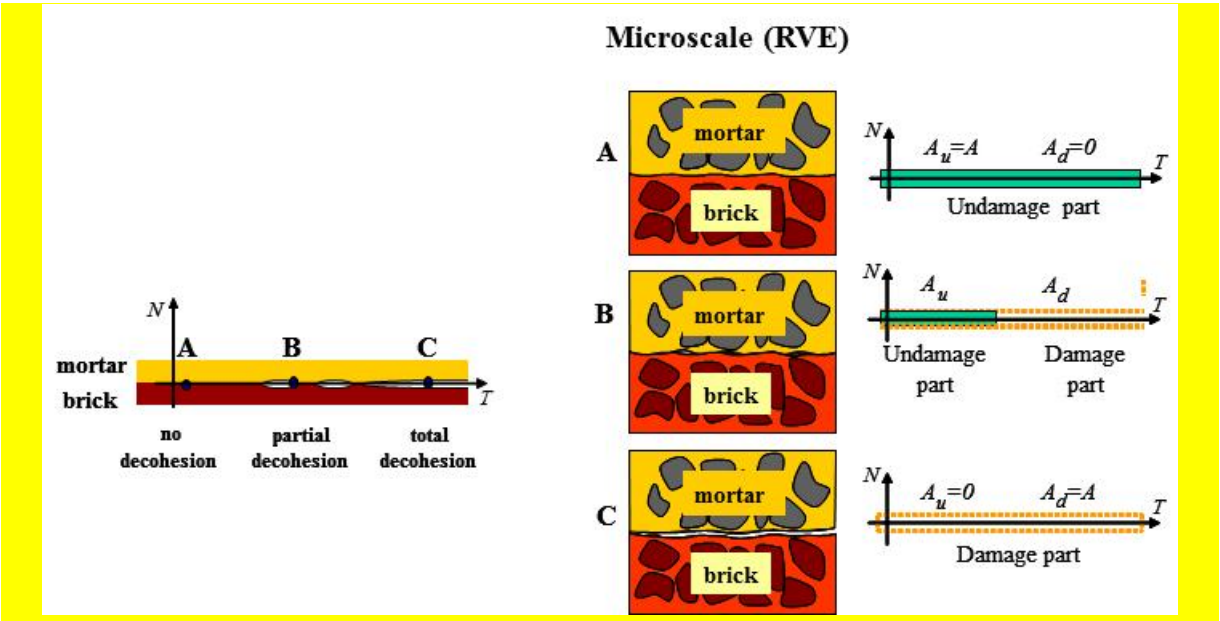

Figure 2: Micromechanical scheme of interface mortar-block.

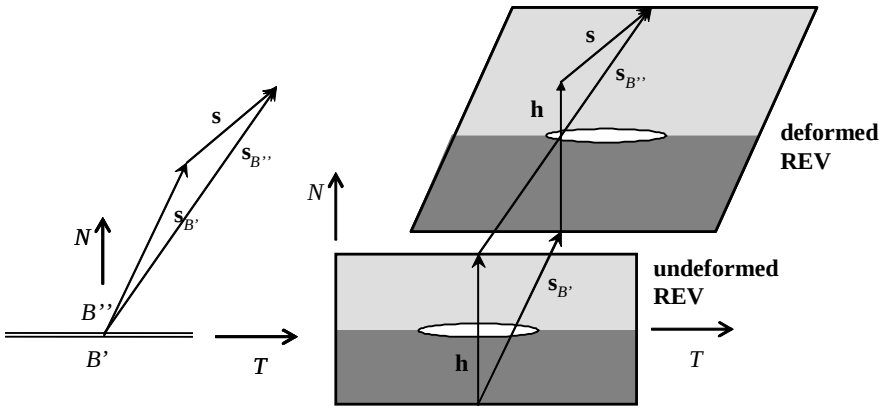

Figure 3: Kinematics at macro- and micro- scale.

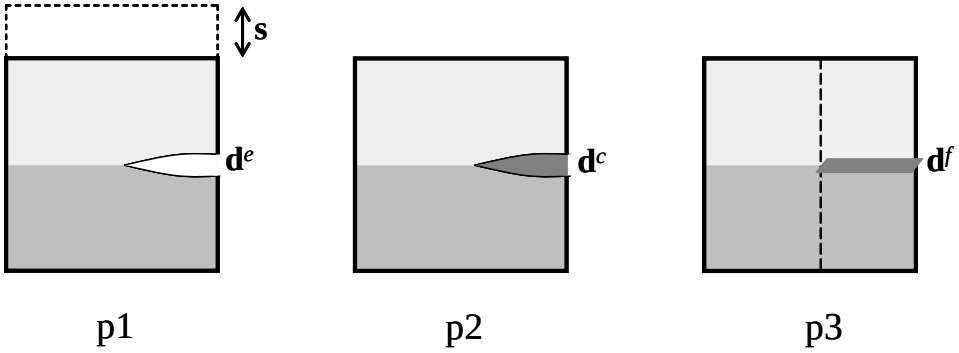

Figure 4: Schemes for the computations.

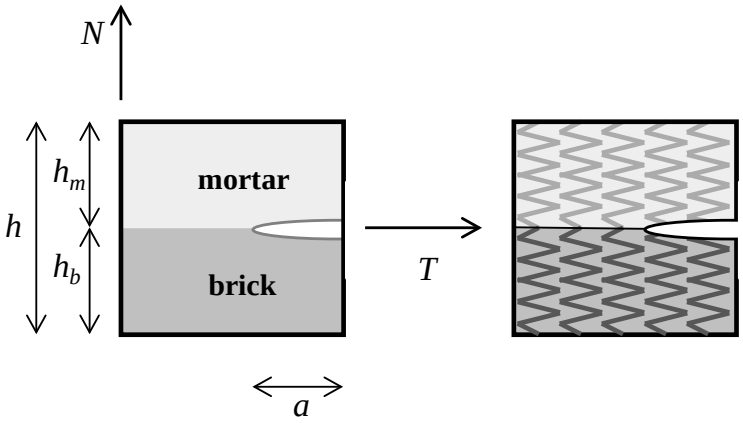

Figure 5: Simplified scheme for the RVE.

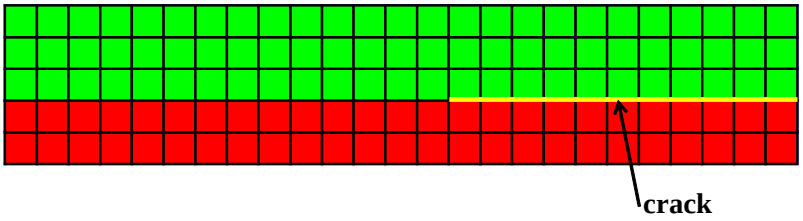

Figure 6: Finite element mesh for the heterogeneous RVE, with microcrack.

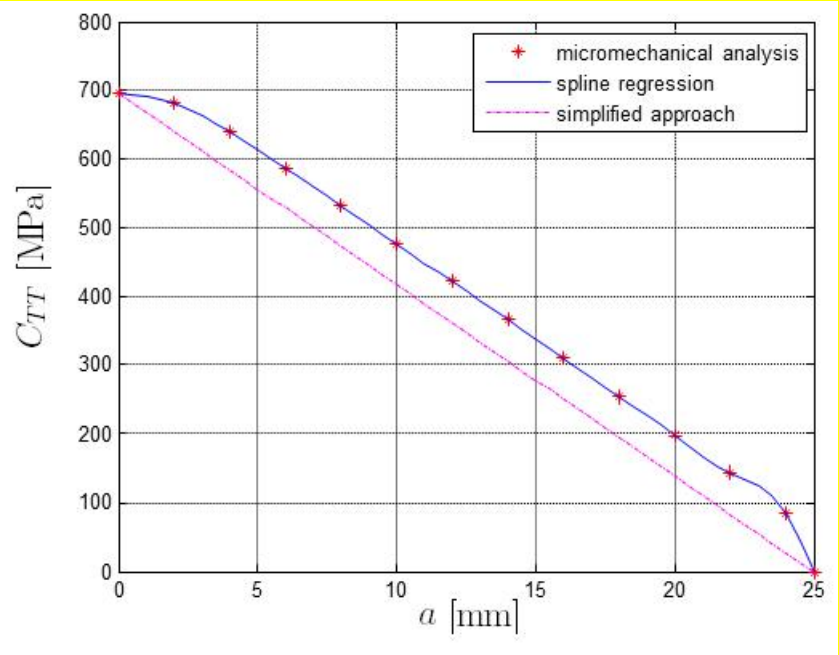

Figure 7: Variation of the overall elastic coefficient C_{TT} as function of the crack length *a*.

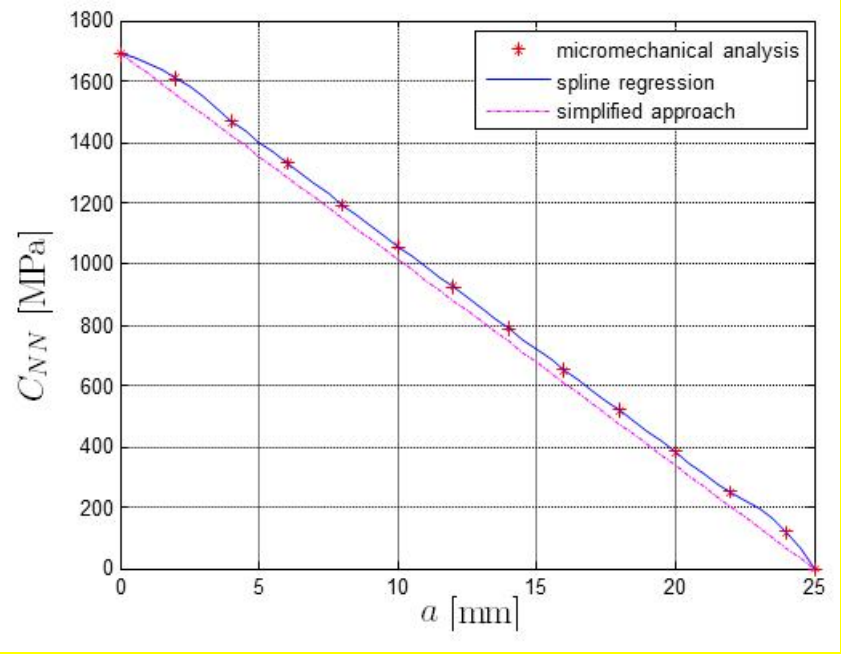

Figure 8: Variation of the overall elastic coefficient C_{NN} as function of the crack length *a*.

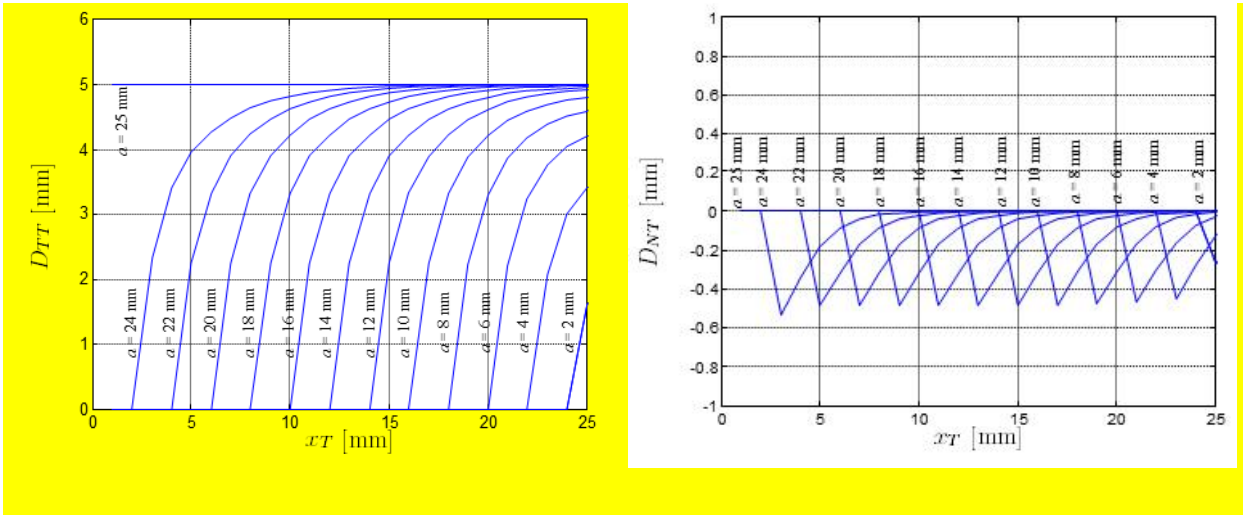

Figure 9: First column of the matrix D versus x_T for different values of the crack length *a*.

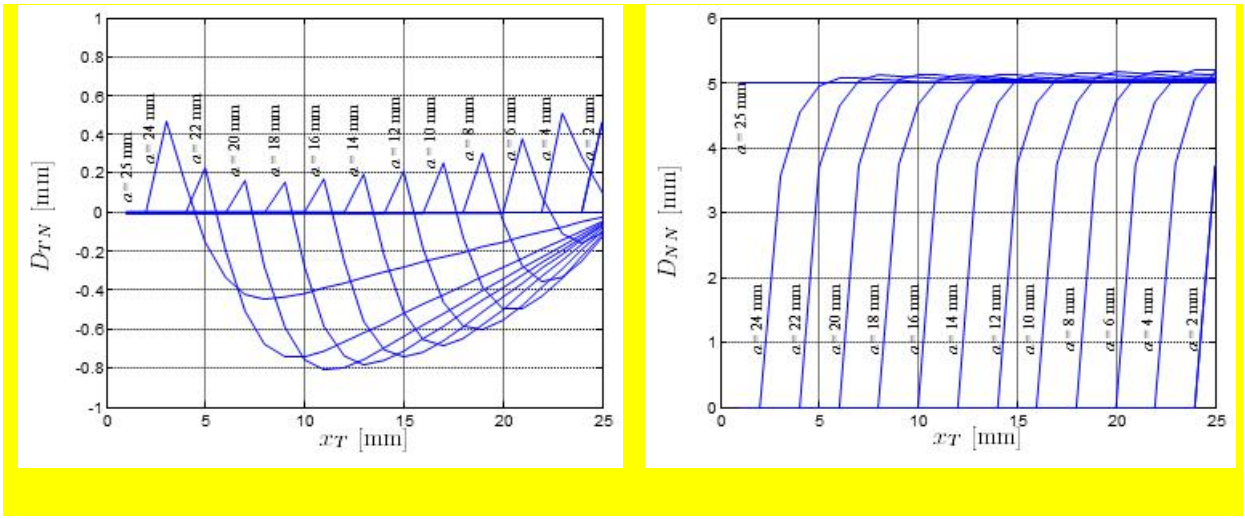

Figure 10: Second column of the matrix D versus x_T for different values of the crack length *a*.

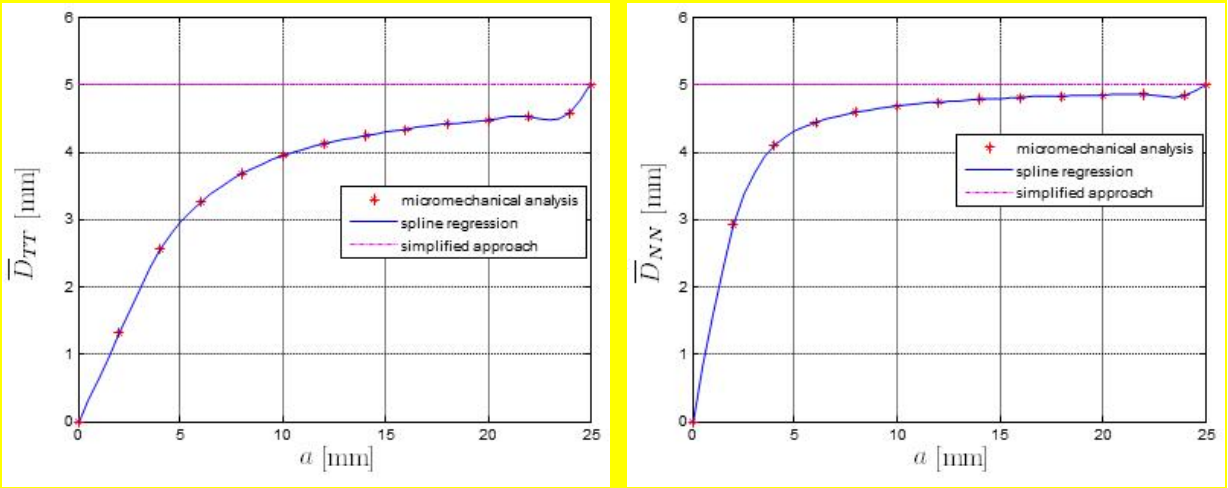

Figure 11: Average values and spline interpolation of $\overline{D}_{TT}$ (a) and $\overline{D}_{NN}$ (b) versus the crack length *a*.

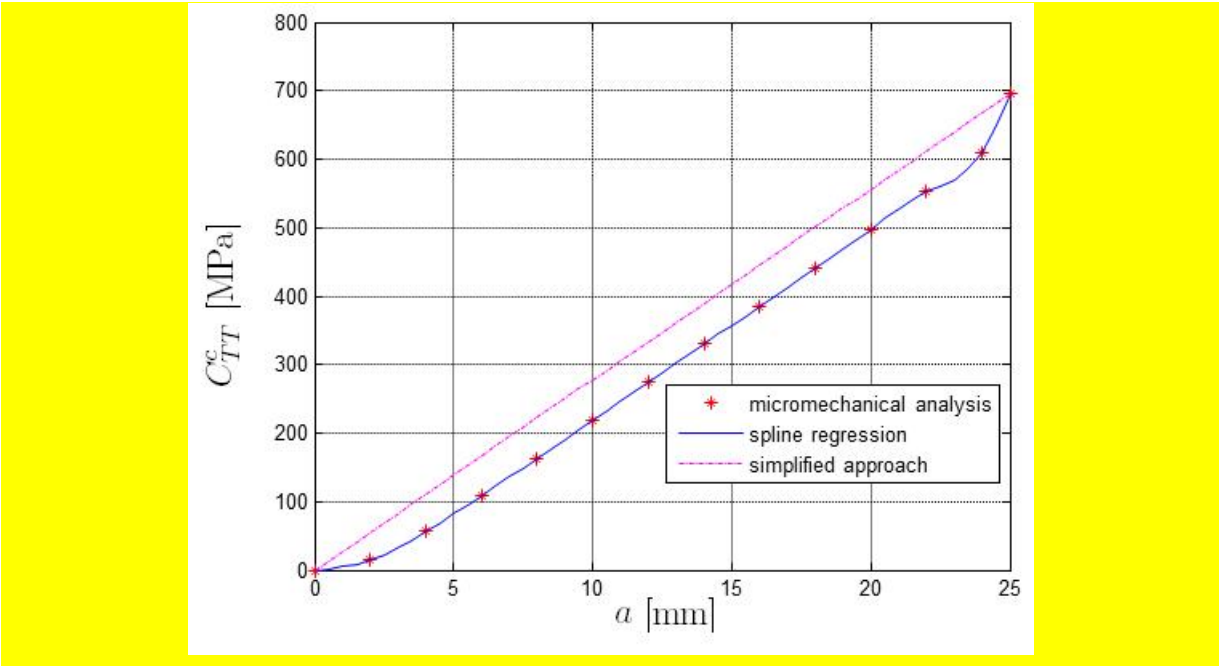

Figure 12: Variation of the overall elastic coefficient C^e_{TT} as function of the crack length *a*.

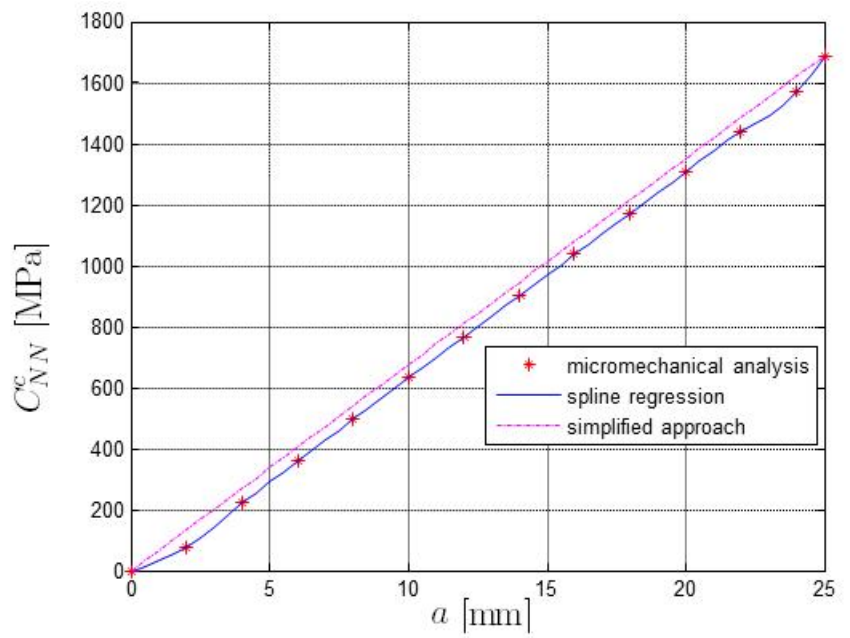

Figure 13: Variation of the overall elastic coefficient C^c_{NN} as function of the crack length a.

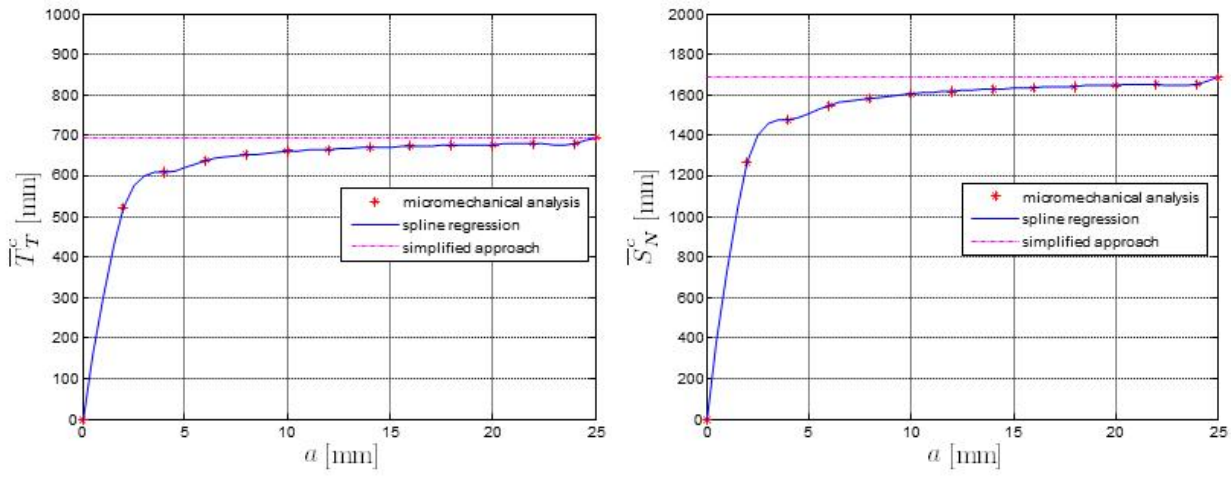

Figure 14: Variation of the contact coefficients T^c_T (a) and S^c_N (b) vs the crack length a.

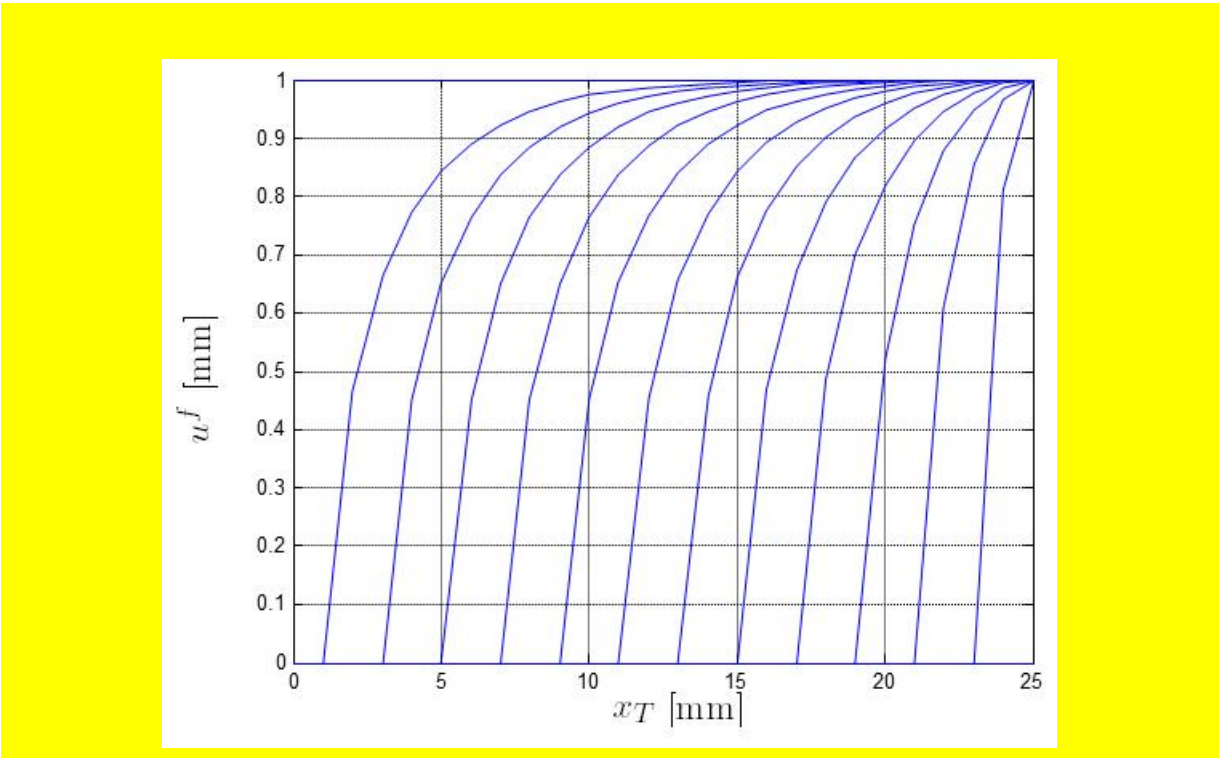

Figure 15: Tangential relative displacement fields u^f to prescribe for each value of the crack length *a*.

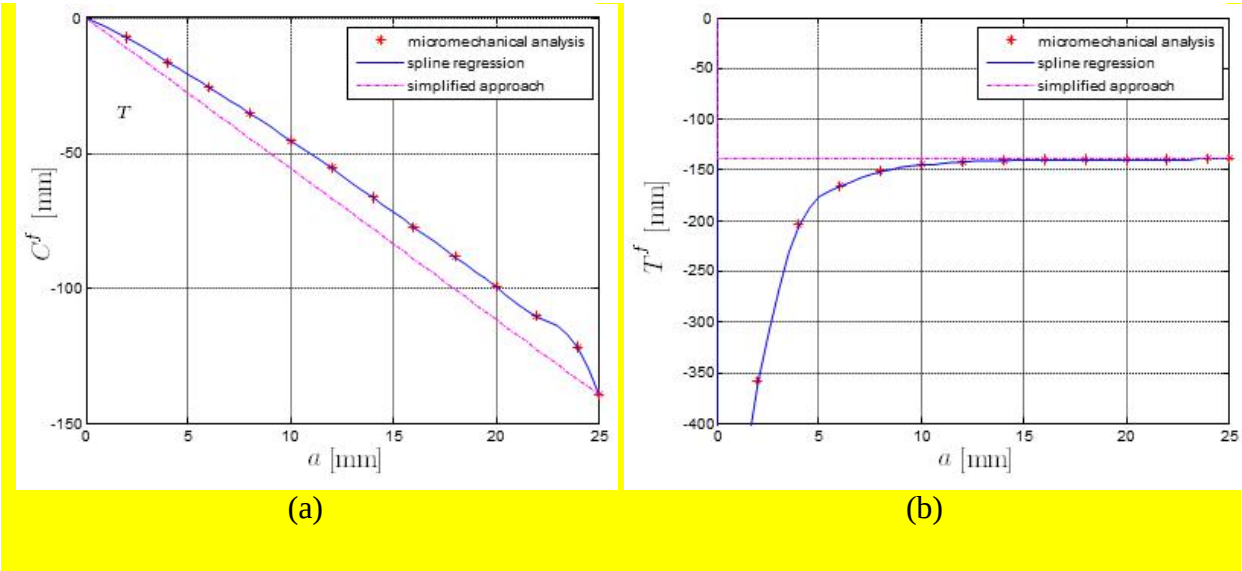

(a) (b)

Figure 16: Variation of the contact stress parameters $C^f{}_T$ (a) and T^f (b) vs the crack length *a*.

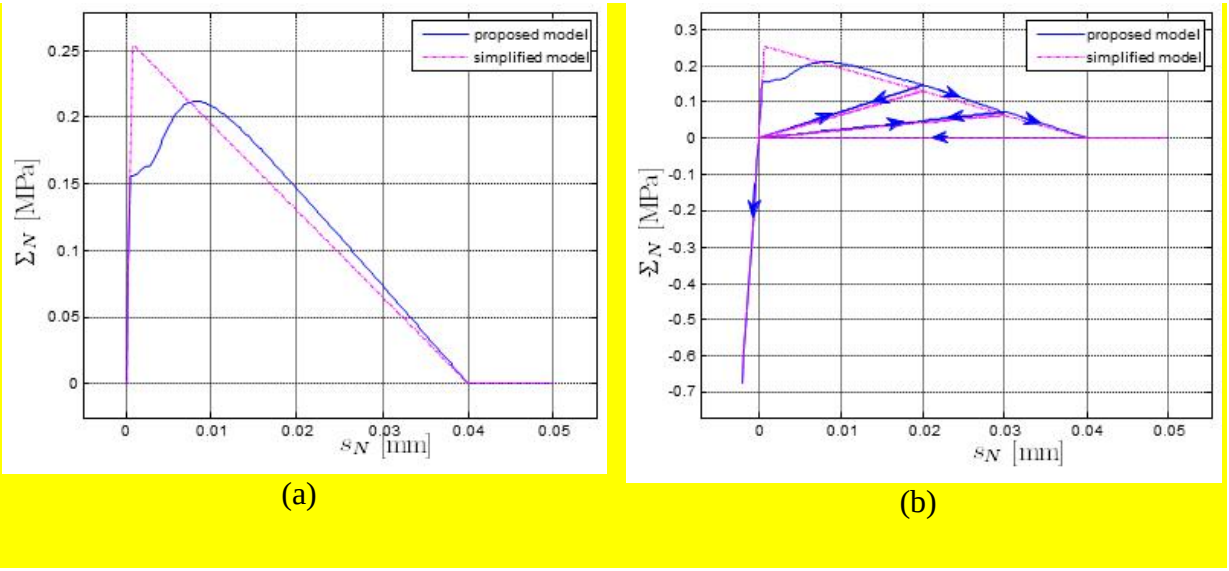

Figure 17: Normal stress vs normal relative displacement for monotonic (a) and cyclic (b) loading conditions.

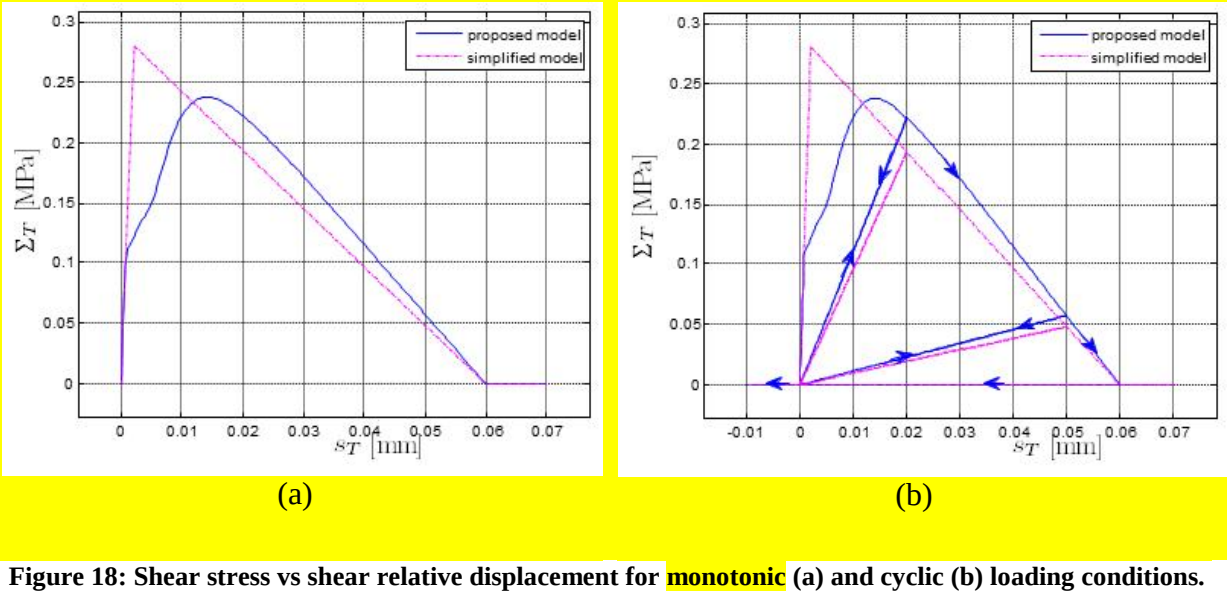

Figure 18: Shear stress vs shear relative displacement for monotonic (a) and cyclic (b) loading conditions.

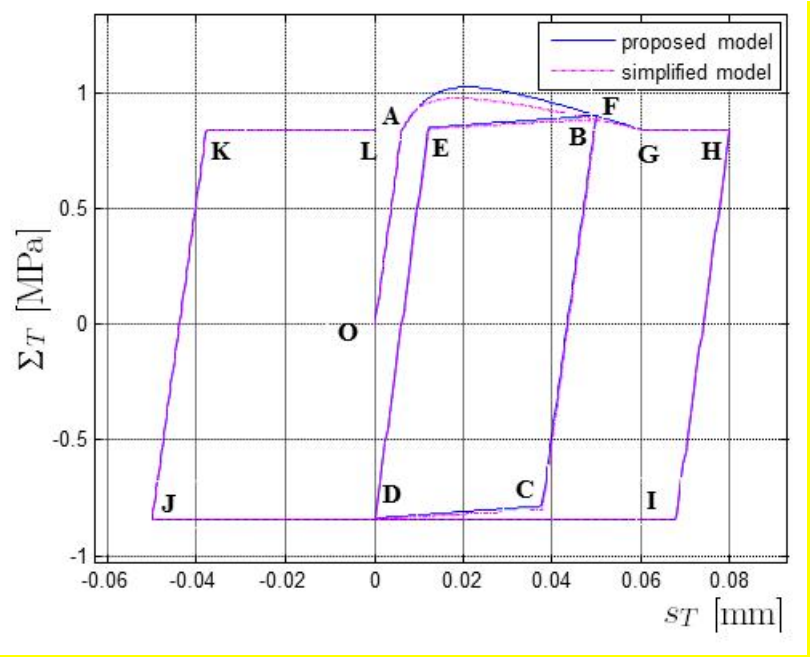

Figure 19: Cyclic loading history for the mixed mode fracture test.

Captions of the Tables

Table 1: Mechanical parameters adopted for the computations.

Table 2: Loading history for mode I of fracture

Table 3: Loading history for mode II of fracture

Table 4: Loading history for mixed mode of fracture

Tables

Table 1: Mechanical parameters adopted for the computations.

$G_{cT} = 0.0085$ Nmm/mm	$s_T^0 = 0.00072$ mm	$s_T^f = 0.06$ mm
$G_{cN} = 0.0050$ Nmm/mm	$s_N^0 = 0.00044$ mm	$s_N^f = 0.04$ mm

Table 2: Loading history for mode I of fracture

	t	0	1	2	3	4	5	6
$h1_I$	s_N [mm]	0	0.05	-	-	-	-	-
	s_T [mm]	0	0	-	-	-	-	-
$h2_I$	s_N [mm]	0	0.02	0	0.03	0	0.05	-0.002
	s_T [mm]	0	0	0	0	0	0	0

Table 3: Loading history for mode II of fracture

	t	0	1	2	3	4	5	6
$h1_{II}$	s_N [mm]	0	0	-	-	-	-	-
	s_T [mm]	0	0.07	-	-	-	-	-
$h2_{II}$	s_N [mm]	0	0	0	0	0	0	0
	s_T [mm]	0	0.02	0	0.05	0	0.07	-0.01

Table 4: Loading history for mixed mode of fracture

t	0	1	2	3	4	5	6
s_N [mm]	-0.005	-0.005	-0.005	-0.005	-0.005	-0.005	-0.005
s_T [mm]	0	0	0.05	0	0.08	-0.05	0